PCCP

ROYAL SOCIETY OF CHEMISTRY

PAPER

View Article Online
View Journal | View Issue

Cite this: *Phys. Chem. Chem. Phys.*, 2022, **24**, 28878

Electron transport *via* tyrosine-doped oligo-alanine peptide junctions: role of charges and hydrogen bonding†

Cunlan Guo, *[af] Yulian Gavrilov, [bg] Satyajit Gupta, [ah] Tatyana Bendikov,[c] Yaakov Levy, [b] Ayelet Vilan, [d] Israel Pecht, [e] Mordechai Sheves [a] and David Cahen [a]

Received 21st June 2022,
Accepted 17th November 2022

DOI: 10.1039/d2cp02807g

rsc.li/pccp

A way of modulating the solid-state electron transport (ETp) properties of oligopeptide junctions is presented by charges and internal hydrogen bonding, which affect this process markedly. The ETp properties of a series of tyrosine (Tyr)-containing hexa-alanine peptides, self-assembled in monolayers and sandwiched between gold electrodes, are investigated in response to their protonation state. Inserting a Tyr residue into these peptides enhances the ETp carried *via* their junctions. Deprotonation of the Tyr-containing peptides causes a further increase of ETp efficiency that depends on this residue's position. Combined results of molecular dynamics simulations and spectroscopic experiments suggest that the increased conductance upon deprotonation is mainly a result of enhanced coupling between the charged C-terminus carboxylate group and the adjacent Au electrode. Moreover, intra-peptide hydrogen bonding of the Tyr hydroxyl to the C-terminus carboxylate reduces this coupling. Hence, the extent of such a conductance change depends on the Tyr-carboxylate distance in the peptide's sequence.

Introduction

Electron transfer (ET) *via* proteins is a key element in biological energy conversion and enzymatic catalysis.[1,2] The structural and chemical properties of a protein's polypeptide matrix play critical roles in electron transfer within as well as between proteins, and in regulating protein functions. The amino acid composition and sequence, length and secondary structure of peptides may all contribute to the their capacity of electron transfer in solution and the electron transport (ETp) presently observed in the solid-state under high vacuum, conditions remote from those of the former[3–8] though some disagreements still exist between certain theoretical calculations and experimental measurements.[9–12] The composition and sequence of amino acids in a peptide determine its frontier orbitals energy levels and molecular dipole, and hence also affect the ETp it carries.[11,13,14] Amino acid compositions of peptides have been investigated for their roles in ETp. Homopeptides, composed of charged lysine (Lys) and glutamic acid (Glu) residues or containing aromatic ones, like tryptophan (Trp), were found to have higher conductance than *e.g.*, oligo-alanine of similar length.[11] The sequence of hetero-peptides has also been found to affect their conductance; for example, replacing one alanine (Ala) in a hepta-Ala junction by a Trp was found to enhance the ETp, and its extent depended on its sequence position, increasing as the Trp was closer to one of the electrodes.[9] Besides that, non-covalent interactions between and within the peptides, responding to the surrounding environments, can also modulate charge transport, which may well be relevant for the protein functions but has not been explored till now.

Tyrosine (Tyr) is an aromatic amino acid with a relatively small HOMO–LUMO gap[15] and a correspondingly low HOMO (with respect to vacuum).[16,17] Like Trp, Tyr participates in diverse catalytic functions of proteins[18–21] also acting as an

[a] *Departments of Molecular Chemistry and Materials Science, Weizmann Institute of Science, Rehovot, 761001, Israel. E-mail: cunlanguo@whu.edu.cn*
[b] *Departments of Chemical and Structural Biology, Weizmann Institute of Science, Rehovot, 761001, Israel*
[c] *Department of Chemical Research Support, Weizmann Institute of Science, Rehovot, 761001, Israel*
[d] *Departments of Chemical & Biological Physics, Weizmann Institute of Science, Rehovot, 761001, Israel*
[e] *Department of immunology and Regenerative Biology, Weizmann Institute of Science, Rehovot, 761001, Israel*
[f] *College of Chemistry and Molecular Sciences, Wuhan University, Wuhan 430072, China*
[g] *Division of Biophysical Chemistry, Center for Molecular Protein Science, Department of Chemistry, Lund University, SE-22100 Lund, Sweden*
[h] *Department of Chemistry, Indian Institute of Technology, Bhilai, 492015, India*
† Electronic supplementary information (ESI) available. See DOI: **https://doi.org/10.1039/d2cp02807g**

electron donor,[22–24] due to its possible redox activity[25] and lower ionization potential than that of non-aromatic amino acids. Like other amino acid residues, Tyr function is also influenced by its surrounding environment and can, accordingly, influence the function of a protein.[26] In the present study, we employed a series of hetero-hepta-peptides where a Tyr residue was inserted at different sequence positions between the C and the N termini, to investigate the role of this residue in ETp in different environments. The fact that both the peptide C-terminus carboxyl and the Tyr phenol can bind or donate a proton in a pH-dependent manner, enabled investigation of the ETp *via* these peptides as a function of their degree of protonation. Solid-state junctions of such hetero-oligopeptide monolayers were constructed between two gold electrodes and studied under neutral or alkaline conditions. Their conductance characteristics were studied in dry condition under vacuum from room down to cryogenic temperatures. Molecular dynamics (MD) simulations, angle-resolved X-ray photoelectron spectroscopy (ARXPS) and UV photoelectron spectroscopy (UPS) provided detailed structural information of the monolayers, and enabled analysis of their frontier orbital energy level changes under different conditions. Polarization modulation–infrared reflection–absorption spectroscopy (PM-IRRAS) gave insight into changes in chemical bonds, expressed in changes in ETp upon peptide (de)protonation. The Tyr phenol residue was shown to significantly modulate the effect of the terminal carboxylate on the peptide's ETp, significantly depending on the Tyr position in the sequence. The combined effects of the carboxylate charge and the Tyr phenol residue on the peptide conductance provide a new strategy of peptide design for the modulation of its electrical properties.

Results and discussion

Peptide and monolayer characterization

Characterization of the peptides and their monolayers is presented first in order to provide the necessary background for rationalizing the following ETp results. Linear heptapeptides were employed, composed of six Ala and one Tyr inserted at different sequence positions, to study the roles played by the aromatic residue and the state of peptide's protonation in ETp *via* its monolayers. The peptides are named Y-1, Y-4, and Y-7, according to the Tyr position away from the N-terminus of the heptapeptide. To produce uniform and oriented monolayers of the above peptides, 3-mercaptopropionic acid (MPA) was covalently added to the peptides' N-terminus, allowing its binding to an Au electrode surface by an Au–S bond (Fig. 1A).

MD served to simulate the conformation of peptide monolayers by constructing 3 × 3 brushes with the S atom of the MPA fixed in the XY plane (Fig. 1B–D). The MD simulations indicated that the peptides are oriented in the monolayers with small tilt angles and adopt a partial β-sheet structure. The thickness of brushes varied slightly among the three peptides (Table S1, ESI†), where the Tyr sequence position affects the Tyr orientation, peptides' length, tilt angle, and

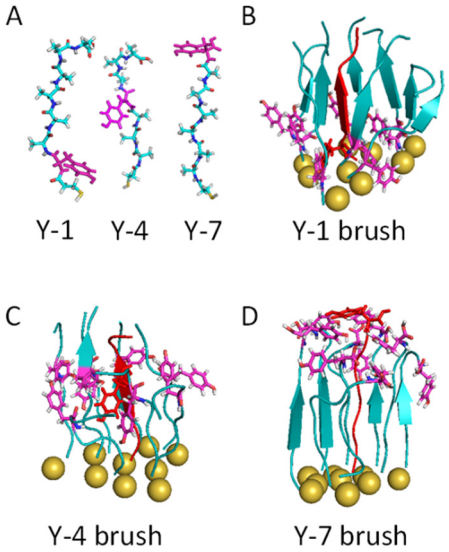

Fig. 1 Peptide structures in different monolayers as evaluated by MD simulations of the 3 × 3 peptide brushes in vacuum. (A) Structure of peptides: Y-1: MPA-YAAAAAA; Y-4: MPA-AAAYAAA; Y-7: MPA-AAAAAAY (A = alanine, Y= tyrosine). 3-Mercapto-propionic acid (MPA) was attached by an amide bond to the N terminus of the peptides. (B)–(D) Peptide brushes of Y-1, Y-4, and Y-7 with only sulfur atoms fixed in one plane. Sulfur atoms are illustrated by the yellow balls, and one peptide backbone is marked in red as an illustration.

β-sheet-like content in the monolayer. For example, the Tyr phenol ring of Y-7 is almost perpendicular to the peptide's backbone and close to the carboxyl of the adjacent C-terminus.

The thicknesses of the Y-peptide monolayers (except Y-1), deduced from ellipsometry, are similar to those of MPA-7Ala (7A) and Trp-doped oligo-alanine (W-peptide) monolayers.[9] The measured thickness is also nearly consistent with the MD results except for that of peptide Y-1 (Table S1, ESI†). The measured thickness of Y-1 is about two thirds of the calculated peptide length. We ascribe this discrepancy to the phenol ring being close to, and possibly interacting with the Au substrate, which interferes with the Au–S bonding-driven peptide assembly and is not accounted for in the MD simulations. The peptides are more stretched and perpendicular to the Au substrate as the Tyr is farther away from the Au substrate, resulting in a larger thickness. This behavior is similar to that of the molecular monolayers formed by Trp-doped hepta-Ala peptides[9] and ferrocene-containing alkylthiols due to the steric hindrance caused by buried substituents forcing a more crumpled conformation.[27]

To investigate the impact of deprotonation on the peptides' monolayer properties and the ETp they carry, the freshly-prepared peptide monolayers were treated by a KOH solution as detailed in the Experimental Section. This treatment caused the monolayer thickness to increase by 5–10 Å, *i.e.*, by 15–50% as detailed in Table S1 (ESI†).

The structural changes of peptide monolayers caused by alkaline deprotonation of Tyr phenol and C-terminus carboxyl were also characterized by PM-IRRAS (Fig. 2 and Fig. S1, ESI†). The neutral peptide monolayers of Y-1, Y-4, and Y-7 displayed

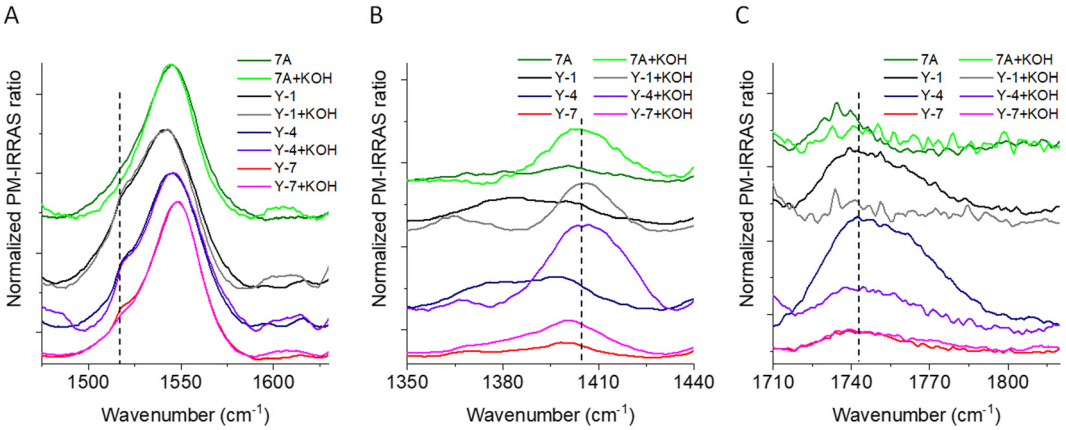

Fig. 2 PM-IRRAS of the peptide monolayers before and after alkaline treatment: 7A, Y-1, Y-4, and Y-7 bound to the Au substrate in the range of (A) 1475–1630 cm^{-1}; (B) 1350–1440 cm^{-1}; (C) 1710–1820 cm^{-1}.

the amide I and II peaks at 1667–1668 and 1541–1548 cm^{-1}, which are similar to the positions of these peaks for 7A (Table S2, ESI†). The amide I mode mainly originates from the C═O stretching vibration and the amide II is mainly due to the N–H in-plane bending and C–N stretching vibrations, which are sensitive to the conformation of the peptide backbone.[28] The amide I/II ratios of Y-4 and Y-7 are similar to that of 7A, which indicates similar conformation of these peptide monolayers, while for Y-1, this ratio is substantially higher, indicating a different conformation. Moreover, a shoulder at 1517 cm^{-1} was observed for all the Tyr-contained peptides, and is assigned to the ν(C═C) of the Tyr phenol ring.[29]

Upon deprotonation, the amide I and II peak positions did not exhibit clear shifts, but the amide I/II intensity ratios of all the peptide monolayers did change. This ratio increased in the order Y-1 > Y-4 > 7A > Y-7, with the increase for Y-7 being substantially lower than that of the others (Fig. S1 and Table S2, ESI†), indicating different extents of conformational changes upon deprotonation. In addition to the amide bonds, the ν(C═C) band intensity of the Tyr phenol ring at 1517 cm^{-1} has also diminished for Y-7, but essentially persisted in Y-1 and Y-4, suggesting the loss of proton from the phenol hydroxyl in Y-7, but not for Y-1 and Y-4 (Fig. 2A).[29] The vibrations at ~1400 cm^{-1} (band of the carboxylate group) were enhanced and those at ~1740 cm^{-1} (feature of the carboxylic group) were attenuated for Y-1, Y-4, and 7A, implying the generation of carboxylate and decrease of carboxylic acid group by deprotonation (Fig. 2B and C). However, for Y-7, such a behavior was not obvious in these two IR ranges.

Taken together, the changes in these three IR ranges reflect the conversion by alkaline treatment of the carboxylic acid groups to carboxylates in peptides having their Tyr relatively distant from the C-terminus (Y-1 and Y-4), and the phenol ring remaining essentially unaffected within these monolayers. When the Tyr residue is close to the C-terminus, as in Y-7, the distinct spectroscopic behavior of the carboxylic and phenol groups suggests that a strong phenolate-carboxyl hydrogen bond is formed, rather than a charged carboxylate group. The proton of the phenol which is shared with the carboxylate and wagging in between,[30] causes the decrease of the tyrosine phenol ring ν(C═C) band amplitude and the persistence of the weak carboxyl group in the PM-IRRAS spectrum following the alkaline treatment.

ARXPS measurements were also carried out following the alkaline treatment and showed similar K/N ratios at different tilt angles (Table S3, ESI†). This established that the potassium ions are uniformly distributed within and above the deprotonated peptide monolayers for balancing their charges. The ratios of K/peptide are about 3 for all the KOH treated Y-peptides and about 2 for the 7A (Fig. S2 and Table S3, ESI†). These values exceed the ratio of K ions to the number of negatively charged residues of carboxylate and phenolate groups per peptide molecule, which may be due to the excess KOH employed in the alkaline treatment, probably yielding potassium carbonate.

Electron transport measurements

The Au-peptide-Au junctions were formed by connecting the peptide monolayers with the bottom microscopic Au electrode and the top tapped gold nanowire (NW), as described in detail previously.[9,11,31] Current–voltage plots of the peptide junctions were measured by applying bias to these junctions. The conductance values of the different peptide monolayers were first measured *via* the neutral ones and found to increase in the order: Y-1 > Y-4 > Y-7 ≈ 7A (Fig. 3A). Taking into consideration the different thickness values of Tyr-doped peptide monolayers, we try to relate the thickness with their observed conductance (Fig. S3, ESI†). Furthermore, we made a length (thickness) normalization of the current values at a given voltage for both the data obtained for the Tyr and the Trp[7] containing peptides (Fig. 3B and Fig. S4, ESI†). The effect of the Tyr sequence position on the conductance was smaller than that observed for the Trp-doped oligo-alanine peptides.[9]

The thickness of the Y-7 monolayer is ~7.7 Å larger than that of the 7A one, but their conductance is similar (Fig. S3, ESI†). In line with these results, the ETp across the three

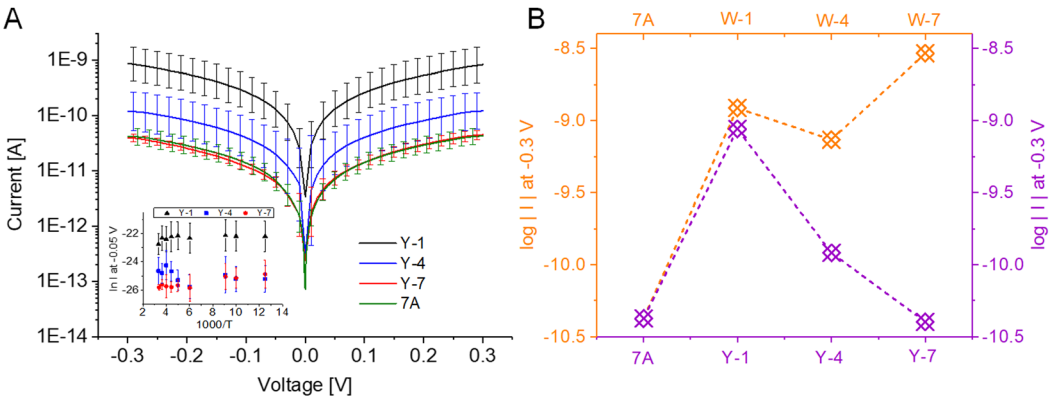

Fig. 3 (A): Semi-log plots of current–voltage characteristics of Au-peptide-Au junctions of neutral Y-1, Y-4, Y-7, and 7A monolayers at 300 K. Each plot is the average of ~20 curves. Inset: Temperature (*T*)-dependence of ln(current) at 50 mV, plotted as function of 1000/*T* (*T* in Kelvin), for Y-1, Y-4, and Y-7 junctions; (B) comparison of currents (at −0.3 V) between Y- (purple with right -axis) and W-peptides (orange with left -axis).

Tyr-doped peptide junctions is higher than that *via* the 7A peptide one. Still, though the Tyr doping increases the currents relative to that *via* 7A junctions (Fig. 3B, purple with right perpendicular-axis) except for Y-7, where the effect is smaller than that *via* the analogous W-doped peptides (Fig. 3B, orange with left *Y*-axis). For example, the conductance of a Y-4 monolayer is about an order of magnitude lower than that *via* the W-4,[9] though Y-4 and W-4 differ in thickness by <1 Å (*i.e.* $<4\%$).

The currents *via* all neutral Tyr peptides at 50 mV showed no temperature dependence in the examined range from 80 K to 300 K (inset of Fig. 3A), which, at the <3.0 nm inter-electrodes' separation distance set by these peptide monolayers, is consistent with electron transport by quantum-mechanical tunneling *via* all of them. Other models for transport can, under specific confluence of circumstances (*e.g.*, in the inverted region of the Marcus model, a model that relies on changes of nuclear coordinates[32,33]), yield lack of significant temperature dependence of current through (bio)molecules. However, none of these models that allow for temperature-independent transport have been tested as thoroughly as the tunneling one (*e.g.*, for small proteins by us[34–37]). Still, true quantum mechanical tunneling requires coherence, and, till now there is only one very recent report[38] with experimental evidence for coherent transport across molecular assemblies.

With tunneling it is plausible that the difference in conductance between Y- and W-doped peptides is due to the lower energy barrier that electrons encounter for ETp across Trp-containing peptide junctions than the Tyr-containing ones. This is in line with the smaller HOMO–LUMO gap[15] and the expected smaller $|\mathrm{HOMO} - E_F|$ barrier (*i.e.* ε_{UPS}, the energy barrier between the peptide's HOMO and the Au Fermi level, determined by UPS, Fig. S5, ESI†) for the W-peptides than for Y-peptides.

We avoid fitting the *I–V* traces to standard tunneling models[39] because the measured *I–V* curves are nearly linear within the limited voltage range (±0.3 V) due to peptide stability (Fig. S7, ESI†). Such linearity implies a single fitting parameter (the slope or conductance) in contrast to two or more free-fitting parameters by various models. Such linearity is possible for *e.g.*, tunneling with energy barrier much larger than maximal applied voltage. Nevertheless, without characteristics trace-features, fitting would be misleading.

The deprotonation of the Tyr-containing peptides was found to cause a significant increase of ETp efficiency that also depended on the Tyr sequence position in the oligopeptide (Fig. 4 and Fig. S3, ESI†). For example, the conductance *via* the deprotonated Y-1 monolayer is 35 times higher than *via* the corresponding protonated Y-1 monolayer. Similarly, the conductance *via* the deprotonated Y-4 monolayer is 18 times higher than *via* the corresponding protonated Y-4 monolayer. Overall, the conductance values after deprotonation followed: Y-1 $>$ Y-4 $\approx$ 7A $>$ Y-7 (Fig. 4A), which is slightly different from that *via* the protonated peptide junctions which is in the order of Y-1 $>$ Y-4 $>$ Y-7 $\approx$ 7A (Fig. 3). Interestingly, the ratio of ETp enhancement *via* deprotonated/protonated peptides monotonically increases as the Tyr position is farther away from the C-terminus: Y-1 $>$ Y-4 $>$ Y-7 (Fig. 4B).

Significantly, the ETp *via* the deprotonated peptide monolayers was also found to be temperature independent over the 80–300 K range; hence, the ETp mechanism taking place *via* the deprotonated peptides' monolayers is also consistent with tunneling (Fig. 4A inset).

The impact of deprotonation on the peptide monolayers' energy barrier, ε_{UPS}, and thereby on their ETp was extracted from the UPS measurements (Fig. 5A). The ε_{UPS} values exhibited small changes upon deprotonation and displayed a qualitative correlation with the current *via* the junctions. The largest $\Delta\varepsilon_{UPS}$ caused by deprotonation was −0.3 eV for 7A, and the largest current enhancement ($\Delta\log|I|$) at −0.3 V caused by deprotonation is more than 1.5 orders of magnitude for 7A, as well. Overall, the ε_{UPS} changes caused by deprotonation showed a kind of zigzag trend as the Tyr is closer to the C-terminus, which does not really follow the trend of current enhancement (Fig. 5B). The variations in ε_{UPS} caused by deprotonation could be mainly due to the carboxyl conversion to carboxylate. Indeed, a relatively large effect is observed for 7A, whereas none is observed for Y-7. This is consistent with the IR results indicating no deprotonation of the Y-7 carboxyl upon alkaline treatment. The

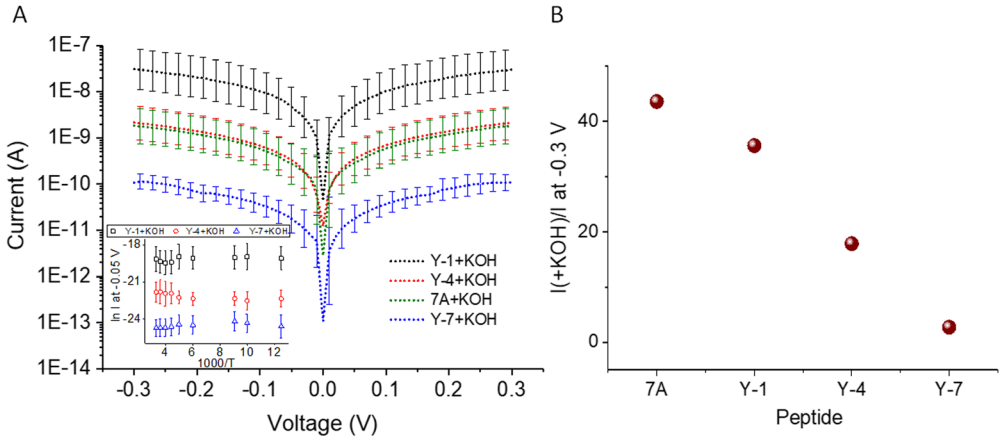

Fig. 4 Electron transport characteristics *via* Au-peptide-Au junctions of Y-1, Y-4, Y-7, and 7A peptides monolayers after deprotonation. (A) Semi-log plots of current–voltage characteristics at 300 K. Each plot is a result of the average of ~20 curves. Inset: Temperature-dependence of ln(current) at 50 mV measured as function of 1000/T (T in K) through Y-1, Y-4, and Y-7 after deprotonation. (B) The ratio of currents monitored after and before alkaline treatment, I(+KOH)/I, measured at −0.3 V as function of the Tyr sequence position.

different effects of carboxyl deprotonation of the Y-peptides on the electronic properties of and transport *via* the monolayers may be due to the hydrogen bonding impact of the tyrosyl hydroxyl. Clearly, this hydrogen bonding capacity is tyrosyl-carboxyl sequence position distance dependent.

Values of the work function (W_F) of the neutral peptide monolayers fluctuated with the Y position in peptide (Fig. S6A, ESI†). This could be due to the peptide dipole moment apart from the Au–S bond, surface polarization effects and/or dipole interactions between peptides.[40–42] Deprotonation of Tyr-containing peptide monolayers caused a 0.25–0.55 eV decrease in absolute W_F value (Fig. S6B, ESI†). This could be due to the negative charges of the carboxylate group pairing with the potassium counterions and possible peptide dipole moment variations in the monolayer following the alkaline treatment.

Thus, while Fig. 5A shows a rough correlation between energy barriers and conductance, additional interactions, including those between the peptide monolayer and the Au NW top electrode also contribute to the ETp, limiting the ability to discern more detailed correlations.

Conductance changes caused by the alkaline treatment also depended on the Tyr position in the peptide sequence. Peptide Y-7 exhibits a distinct behavior as the treatment did hardly affect its conductance. As noted above, the PM-IRRAS data suggest that when the Tyr is proximal to the C-terminus, as in Y-7, a phenolate-carboxyl hydrogen bond is present, competing with the formation of a carboxylate ion. Further comparison of the above spectroscopic data with the conductance results, clearly suggests that the current increase caused by deprotonation is related to the formation of the carboxylate group in the other peptides. In STM-based break-junction measurements of peptides, which require in particular a sufficiently strong molecule–electrode interaction to produce effective Au-peptide-Au junctions, it has been observed that in addition to the electrode-bonding thiol group, only neutral amine and

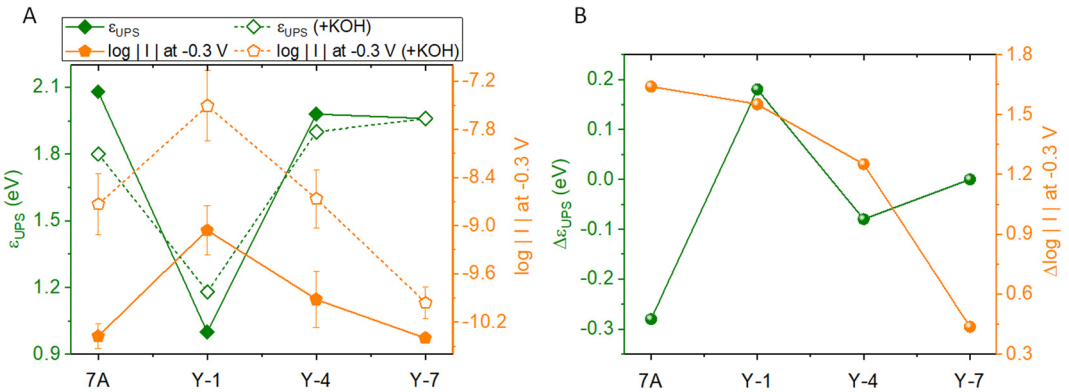

Fig. 5 The energy barriers of peptide monolayers on Au surface compared with the currents they carry. The current *via* the junctions was extracted from the current–voltage curves at −0.3 V. (A) The measured energy barriers (green with left -axis) of the different peptides having distinct Tyr sequence positions, compared with their corresponding current values (orange with the right -axis). The solid and hollow dots are results obtained before and after alkaline treatment, respectively. (B) The differences in energy barriers of the different peptides caused by alkaline treatment (green with the left -axis) compared with the respective current increases (orange with the right -axis). $\Delta\varepsilon_{UPS} = \varepsilon_{UPS}(+KOH) - \varepsilon_{UPS}$, and $\Delta\log|I| = \log|I|(+KOH) - \log|I|$ at −0.3 V.

negatively charged carboxylate groups can help performing valid peptide break-junction measurements.[13] This suggests that an enhanced interaction exists between the peptides' C-terminus carboxylate and the top Au electrode, which can increase the peptide-top Au electrode coupling and enhance the ETp. Since the phenol of Tyr of Y-7 can inhibit deprotonation of the carboxyl group by a hydrogen bond forming with it, coupling to the top electrode is reduced and a lower current is observed. Our finding agrees with a proposal that in a non-polar environment (of the peptide monolayer),[30] it is the carboxylate of the Tyr phenol-carboxyl pair that is protonated and the Tyr phenol is deprotonated, forming a hydrogen bond. For the other two peptides (Y-4, Y-1), where the carboxyl group distance from the Tyr increases, phenol-carboxyl hydrogen bond formation is not plausible. Hence, the carboxyl group is more easily deprotonated, enhancing the coupling with the top electrode. Therefore, these peptides display a conductance increase following deprotonation in the sequence of 7A > Y-1 > Y-4 > Y-7. However, the monolayer thickness order is also affected by deprotonation, as follows: Y-7 ≈ Y-4 ≈ 7A > Y-1 (Table S1 and Fig. S3, ESI†). On the other side, the similar conductance *via* Y-4 and 7A following the deprotonation suggests that the presence of Tyr is not the main factor for conductance change (Fig. 5). Combined with the absence of the deprotonation effect on the conduction *via* Y-7 (Fig. 5), it suggests that the dominant parameter determining the conductance is the carboxylate-electrode coupling (Fig. S3, ESI†).

A detailed recent study carried out measurements of intrinsic electronic conductivity of individual amyloid protein crystals as a model system using a four-electrode approach, which allowed to eliminate contact resistance effects. It has shown an additional, different role of hydrogen bonds in ETp, namely the importance of proton-coupled electron transfer, specifically the role of a proton acceptor, a glutamine, forming a hydrogen bond with a proximal tyrosine in the process.[20]

Experimental

Chemicals

All peptides with a 3-mercaptopropionic acid (MPA) attached at their C-terminus were supplied by GL Biochem Ltd and Hylabs Ltd with purity >95% (HPLC) and were used without further purification. Peptides Y-1, Y-4, and Y-7 were dissolved in acetonitrile water mixture in a 1 : 3 ratio and 7A in the ratio of 3 : 1. The peptides' solution concentration employed for monolayers preparation was ~0.25 mM.

Preparation of peptide monolayers

Au substrates (50 nm in thickness) were treated by plasma for 5 min under the 1 : 1 Ar and O_2 flow after sonication in water and ethanol for 5 min, respectively. The Au substrates were then treated by hot ethanol for ~20 min. After another O_3/UV treatment for 10 min, the Au substrates were immediately incubated in the peptide solution for 48 h. Afterwards, the Au substrates were rinsed with acetonitrile : H_2O (1 : 3) mixture and ethanol followed by dry nitrogen.

Alkaline treatment of the peptide monolayers took place after producing the neutral peptide monolayers by 48 h incubation of the Au substrates in the peptides' solution. Then, a required volume of 1 M KOH aqueous solution was added to the neutral peptide solution in order to adjust it into a 10 mM KOH. The Au substrates were still kept in this alkaline peptide solution for another 1 h incubation. The Au substrates carrying the bound peptide monolayers were then washed with a 10 mM KOH in acetonitrile : H_2O (1 : 3) mixture and dried by flowing nitrogen for 1–2 minutes.

Ellipsometry measurements

A multiple-wavelength ellipsometer (Woollam M-2000 V) was employed at an angle of incidence of 70° to measure the ellipsometry of the peptide monolayers on Au substrate. The Cauchy model was used to evaluate the thickness of the peptide monolayers on the Au substrate.

Molecular dynamics (MD) simulations

The all-atom MD simulations using the GROMACS package Version 4.5.4[43] and the CHARMM force field[44] were used to study the conformation of the peptide monolayers. A 3 × 3 array with only the sulfur atom fixed in the XY plane was constructed to simulate the monolayer. The simulations were set in vacuum to mimic the dry environment of peptide monolayer. All the peptides were simulated for 100 ns in order to ensure achieving equilibration.

Au-peptide-Au junction construction

The junctions were prepared as previously reported.[31] Peptide monolayers were first assembled on the microscopic electrodes. Then, using dielectrophoresis, the Au NWs were trapped between two microscopic electrodes at an AC voltage of 1.5 V, 1 MHz for 5 min. The formed junctions were then rinsed by ethanol and dried by nitrogen. Optical microscopy was used to inspect the trapped NWs. Usually, only one NW bridged the two electrodes, and only those with clear NW bridges were selected for measurements. The nature of the dielectrophoretic trapping process is such that one of the two contacts, likely the one on which the NW "lands" first, is nearly always shorted so that only a single junction remains for ETp measurement.[11,31]

Current–voltage characterization

For ETp measurements, a DC bias was applied between the two microscopic electrodes, with the substrate as ground. For statistics, more than 100 junctions were recorded on 2 to 4 different microscopic-electrode chips.

Temperature dependence of the current–voltage

For each studied peptide, ~20 junctions of the chip, at the center of the distribution, were selected for measurements of the current-temperature dependence. The sample's temperature was controlled in high vacuum, using a TTPX cryogenic electrical measurement system (Lakeshore). The samples were

measured at the set temperature when the sample and probes reached the corresponding thermal equilibrium. The accuracy for temperature control and measurement was 0.2 K.

Ultraviolet photoemission spectroscopy (UPS)

A Kratos AXIS ULTRA system with a concentric hemispherical electron energy analyzer for photo-emitted electron detection was employed to collect UPS data of the peptide monolayers. The source was a He discharge lamp, using He I (21.22 eV) radiation lines. The energy resolution was better than 100 meV, as determined by the Fermi edge of an Au reference sample. We used the logarithmic intensity scale to determine the HOMO edge by extrapolation to the background signal level. The results, obtained in this way, were not significantly different from those obtained using extrapolation on a linear intensity scale.

Angle-resolved X-ray photoelectron spectroscopy (ARXPS)

The same system employed for UPS measurements, using a monochromatized Al Kα X-ray source at 75 W, was used for the XPS data collection. Three take-off angles of 0°, 45°, and 65°, which are the angles between the axis of the analyzer and the normal to the substrate surface, were set to examine the distribution of the K^+ ions in the deprotonated peptide monolayers.

Polarization modulation-infrared reflection-absorption spectroscopy (PM-IRRAS)

A Nicolet 6700 FTIR spectrometer coupled with a PEM-90 photoelastic modulator (Hinds Instruments, Hillsboro, OR) was used to collect PM-IRRAS data of the peptide monolayers on the Au with an incident angle of 80° and a resolution of 2 cm^{-1}. The IR signal was recorded with an MCT-A detector.

Conclusions

In summary, the impact of replacing an Ala residue in a hepta-Ala peptide by a Tyr on the ETp *via* junctions of these peptides' monolayers has been investigated. Temperature independence of the conductance *via* these junctions is consistent with electron transport by super-exchange-mediated quantum tunneling. The inserted Tyr was found to enhance ETp compared to that *via* 7A monolayers, but less than does Trp insertion. This can be rationalized by the larger delocalized π–π orbitals of the Trp indole side chain than that of the phenol in Tyr. Increased aromaticity will decrease the HOMO–LUMO gap. Given that the electrode Fermi level will be within that gap, higher aromaticity will lower the barrier to current flow *via* the peptide, which is determined by the smallest of the energy differences between electrode Fermi level and HOMO or LUMO. Furthermore, the state of protonation of the Tyr-containing peptides was found to affect the electrical conductance of their junctions. The influence of alkaline treatment on ETp *via* the Tyr-doped peptide junctions depended on the Tyr sequence position. Upon deprotonation, the coupling with the Au electrode is markedly enhanced for most of the Tyr-containing peptides, probably by the enhanced interaction of the charged C-terminal carboxylate with the top Au electrode. We explain the exceptional behavior of the Y-7 peptide by the formation of a phenol-carboxyl hydrogen bond enabled by their proximity, which competes with the carboxylate–Au interaction. Thus, hydrogen bonding through intra-peptide side chain interaction can regulate the electrical transport properties of the monolayers. This result represents a hitherto unexplored way of employing hetero-oligopeptides' structure for controlling electronic transport properties of biomolecular junctions.

Conflicts of interest

The manuscript was written through contributions of all authors. All authors have given approval to the final version of the manuscript. There are no conflicts to declare.

Acknowledgements

C. G. thanks the NSFC (21974102 and 21705019) for financial support, and the Weizmann Institute for a senior P. D. fellowship. D. C. and M. S. thank the Israel Science Foundation for financial support. M. S. thanks the Kimmelman Center for Biomolecular Structure and Assembly for partial support. The research is made possible in part by the historic generosity of the Harold Perlman family. M. S. holds the Katzir-Makineni Chair in Chemistry.

Notes and references

1 H. B. Gray and J. R. Winkler, *Annu. Rev. Biochem.*, 1996, **65**, 537–561.
2 H. B. Gray and J. R. Winkler, *Q. Rev. Biophys.*, 2003, **36**, 341–372.
3 N. Amdursky, *ChemPlusChem*, 2015, **80**, 1075–1095.
4 J. Juhaniewicz, J. Pawlowski and S. Sek, *Isr. J. Chem.*, 2015, **55**, 645–660.
5 A. Shah, B. Adhikari, S. Martic, A. Munir, S. Shahzad, K. Ahmad and H.-B. Kraatz, *Chem. Soc. Rev.*, 2015, **44**, 1015–1027.
6 H. Zheng, F. Jiang, R. He, Y. Yang, J. Shi and W. Hong, *Chin. J. Chem.*, 2019, **37**, 1083–1096.
7 J. Yu, J. R. Horsley and A. D. Abell, *Phys. Chem. Chem. Phys.*, 2020, **22**, 8409–8417.
8 B. Zhang, W. Song, J. Brown, R. Nemanich and S. Lindsay, *J. Am. Chem. Soc.*, 2020, **142**, 6432–6438.
9 C. Guo, X. Yu, S. Refaely-Abramson, L. Sepunaru, T. Bendikov, I. Pecht, L. Kronik, A. Vilan, M. Sheves and D. Cahen, *Proc. Natl. Acad. Sci. U. S. A.*, 2016, **113**, 10785–10790.
10 W. M. Schosser, L. A. Zotti, J. Carlos Cuevas and F. Pauly, *J. Chem. Phys.*, 2019, **150**, 174705.
11 L. Sepunaru, S. Refaely-Abramson, R. Lovrincic, Y. Gavrilov, P. Agrawal, Y. Levy, L. Kronik, I. Pecht, M. Sheves and D. Cahen, *J. Am. Chem. Soc.*, 2015, **137**, 9617–9626.

12 L. A. Zotti and J. C. Cuevas, *ACS Omega*, 2018, **3**, 3778–3785.
13 J. M. Brisendine, S. Refaely-Abramson, Z.-F. Liu, J. Cui, F. Ng, J. B. Neaton, R. L. Koder and L. Venkataraman, *J. Phys. Chem. Lett.*, 2018, **9**, 763–767.
14 J. Juhaniewicz and S. Sek, *J. Electroanal. Chem.*, 2010, **649**, 83–88.
15 M. Granold, P. Hajieva, M. I. Toşa, F.-D. Irimie and B. Moosmann, *Proc. Natl. Acad. Sci. U. S. A.*, 2018, **115**, 41–46.
16 P. H. Cannington and N. S. Ham, *J. Electron Spectrosc. Relat. Phenom.*, 1979, **15**, 79–82.
17 E. W. Schlag, S.-Y. Sheu, D.-Y. Yang, H. L. Selzle and S. H. Lin, *Angew. Chem., Int. Ed.*, 2007, **46**, 3196–3210.
18 H. B. Gray and J. R. Winkler, *Proc. Natl. Acad. Sci. U. S. A.*, 2015, **112**, 10920–10925.
19 O. B. Morozova, A. V. Yurkovskaya, A. S. Kiryutin, L. A. Yarinich, V. N. Silnikov and R. Z. Sagdeev, *Dokl. Phys. Chem.*, 2013, **452**, 233–238.
20 C. Shipps, H. R. Kelly, P. J. Dahl, S. M. Yi, D. Vu, D. Boyer, C. Glynn, M. R. Sawaya, D. Eisenberg, V. S. Batista and N. S. Malvankar, *Proc. Natl. Acad. Sci. U. S. A.*, 2021, **118**, e2014139118.
21 C. Wittekindt, M. Schwarz, T. Friedrich and T. Koslowski, *J. Am. Chem. Soc.*, 2009, **131**, 8134–8140.
22 M. Cordes, A. Koettgen, C. Jasper, O. Jacques, H. Boudebous and B. Giese, *Angew. Chem., Int. Ed.*, 2008, **47**, 3461–3463.
23 J. A. Gao, P. Muller, M. Wang, S. Eckhardt, M. Lauz, K. M. Fromm and B. Giese, *Angew. Chem., Int. Ed.*, 2011, **50**, 1926–1930.
24 M. Wang, J. Gao, P. Muller and B. Giese, *Angew. Chem., Int. Ed.*, 2009, **48**, 4232–4234.
25 J. Lee, M. Ju, O. H. Cho, Y. Kim and K. T. Nam, *Adv. Sci.*, 2019, **6**, 1801255.
26 A. Nilsen-Moe, C. R. Reinhardt, S. D. Glover, L. Liang, S. Hammes-Schiffer, L. Hammarström and C. Tommos, *J. Am. Chem. Soc.*, 2020, **142**, 11550–11559.
27 L. Yuan, N. Nerngchamnong, L. Cao, H. Hamoudi, E. del Barco, M. Roemer, R. K. Sriramula, D. Thompson and C. A. Nijhuis, *Nat. Commun.*, 2015, **6**, 6324.
28 A. Barth, *Biochim. Biophys. Acta, Bioenerg.*, 2007, **1767**, 1073–1101.
29 A. Barth, *Prog. Biophys. Mol. Biol.*, 2000, **74**, 141–173.
30 B. Koeppe, J. Guo, P. M. Tolstoy, G. S. Denisov and H.-H. Limbach, *J. Am. Chem. Soc.*, 2013, **135**, 7553–7566.
31 G. Noy, A. Ophir and Y. Selzer, *Angew. Chem., Int. Ed.*, 2010, **49**, 5734–5736.
32 Y. Han, C. Nickle, M. S. Maglione, S. K. Karuppannan, J. Casado-Montenegro, D.-C. Qi, X. Chen, A. Tadich, B. Cowie, M. Mas-Torrent, C. Rovira, J. Cornil, J. Veciana, E. del Barco and C. A. Nijhuis, *Adv. Sci.*, 2021, **8**, 2100055.
33 L. Yuan, L. Wang, A. R. Garrigues, L. Jiang, H. V. Annadata, M. Anguera Antonana, E. Barco and C. A. Nijhuis, *Nat. Nanotechnol.*, 2018, **13**, 322–329.
34 J. A. Fereiro, T. Bendikov, I. Pecht, M. Sheves and D. Cahen, *J. Am. Chem. Soc.*, 2020, **142**, 19217–19225.
35 J. A. Fereiro, B. Kayser, C. Romero-Muniz, A. Vilan, D. A. Dolgikh, R. V. Chertkova, J. C. Cuevas, L. A. Zotti, I. Pecht, M. Sheves and D. Cahen, *Angew. Chem., Int. Ed.*, 2019, **58**, 11852–11859.
36 J. A. Fereiro, G. Porat, T. Bendikov, I. Pecht, M. Sheves and D. Cahen, *J. Am. Chem. Soc.*, 2018, **140**, 13317–13326.
37 B. Kayser, J. A. Fereiro, R. Bhattacharyya, S. R. Cohen, A. Vilan, I. Pecht, M. Sheves and D. Cahen, *J. Phys. Chem. Lett.*, 2020, **11**, 144–151.
38 P. A. Li and Y. Selzer, *Nat. Commun.*, 2022, **13**, 4742.
39 R. L. McCreery, *Acc. Chem. Res.*, 2022, **55**, 2766–2779.
40 G. Heimel, L. Romaner, J. L. Bredas and E. Zojer, *Phys. Rev. Lett.*, 2006, **96**, 196806.
41 J. B. Neaton, M. S. Hybertsen and S. G. Louie, *Phys. Rev. Lett.*, 2006, **97**, 216405.
42 F. Rissner, D. A. Egger, A. Natan, T. Koerzdoerfer, S. Kuemmel, L. Kronik and E. Zojer, *J. Am. Chem. Soc.*, 2011, **133**, 18634–18645.
43 B. Hess, C. Kutzner, D. van der Spoel and E. Lindahl, *J. Chem. Theory Comput.*, 2008, **4**, 435–447.
44 N. Foloppe and A. D. MacKerell, *J. Comput. Chem.*, 2000, **21**, 86–104.